https://doi.org/10.15407/ujpe66.1.69

A.S. VDOVYCH,[1] I.R. ZACHEK,[2] R.R. LEVITSKII[1]

[1] Institute for Condensed Matter Physics, Nat. Acad. of Sci. of Ukraine
(1, Svientsitsky Str., Lviv 79011, Ukraine)
[2] National University "Lviv Polytechnic"
(12, Stepan Bandera Str., Lviv 79013, Ukraine; e-mail: zachek_i@ukr.net)

INFLUENCE OF THE STRESSES σ_5 AND σ_6 AND THE ELECTRIC FIELD E_1 ON THE THERMODYNAMIC PARAMETERS OF GPI FERROELECTRIC MATERIALS

Effects arising in glycine phosphite (GPI) ferroelectrics under the action of the shear stresses σ_5 and σ_6 and the electric field E_1 have been studied in the framework of a modified model that accounts for the piezoelectric coupling between the ordered structural elements and the strains ε_j. The components of the polarization vectors and the tensor of static dielectric permittivity are calculated in the two-particle cluster approximation for mechanically clamped crystals. The corresponding piezoelectric and thermal parameters are also determined. The influence of the simultaneous action of the stress σ_5 and the field E_1, as well as the stress σ_6 and the field E_1, on the physical parameters of the GPI ferroelectric crystals and the phase transition in them is analyzed.

Keywords: ferroelectrics, phase transition, dielectric permittivity, piezoelectric moduli, shear stress.

1. Introduction

The study of the phenomena that arise under the action of mechanical stresses and external electric fields is one of the challenging problems in the physics of ferroactive compounds. In particular, it concerns the crystals of glycine phosphite (GPI), which belongs to ferroactive materials with hydrogen bonds [1].

The influence of the transverse electric field E_1 on the dielectric permittivity ε_{33} of a GPI crystal was experimentally studied in works [2–4]. The cited authors showed that the application of the field E_1 resulted in a decrease of the ferroelectric phase transition temperature.

The model of a deformed GPI crystal was developed in work [5] on the basis of the proton model [3]. It considers the piezoelectric coupling between a proton and lattice subsystems. This model served as a basis to study the influence of the transverse electric fields E_1 and E_3 on the dielectric and piezoelectric properties of GPI [6]. In particular, the above-mentioned experimental data obtained for the temperature dependence of the transverse dielectric permittivity ε_{33} in the presence of the field E_3 [3] were described correctly at the quantitative level. It was found that the influence of the field E_1 is qualitatively similar to that of the field E_3, but it is an order of magnitude weaker.

In work [7], the GPI model [6] was modified to describe the case where the shear stresses σ_4, σ_5, and σ_6 are applied to the GPI crystal in the absence of an electric field. It was found that the appearance of the shear stress σ_4 or σ_6 in the ferroelectric phase gives rise to the emergence of the spontaneous polarization along the axes OX and OZ, and the transverse permeabilities ε_{11} and ε_{33} tend to infinity at the temperature T_c. The stresses σ_4 and σ_6 were found to produce similar effects at the qualitative level.

In this work in the framework of a modification of the model [4] of a deformed GPI crystal, the mutual action of the electric field E_1 and the stresses σ_5 and σ_6 on the phase transition in the crystals of this type and their thermodynamic and static dielectric parameters are studied.

2. Model Hamiltonian

Let us consider a system of protons that move in the GPI crystal along the O–H, ..., O bonds. The latter form zigzag chains along the c-axis of the crys-

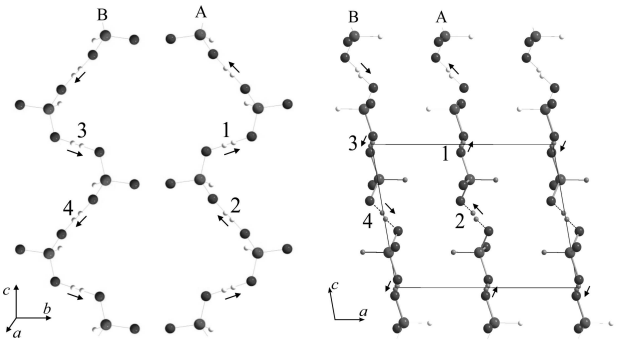

Fig. 1. Orientations of the vectors $\mathbf{d}_{qf}$ in a primitive cell R_s of the ferroelectric phase

tal. Let us assign the dipole moment $\mathbf{d}_{qf}$ to the proton at the f-th bond ($f = 1, ..., 4$). In the ferroelectric phase, the dipole moments are mutually compensated ($\mathbf{d}_{q1}$ with $\mathbf{d}_{q3}$ and $\mathbf{d}_{q2}$ with $\mathbf{d}_{q4}$) in the Z- and X-directions but simultaneously mutually added in the Y-direction, thus generating a spontaneous polarization. The vectors $\mathbf{d}_{qf}$ are oriented at certain angles with respect to the crystallographic axes and have the longitudinal and transverse components with respect to the b-axis (see Fig. 1).

The Hamiltonian of the proton subsystem in GPI consists of the "seed" and pseudospin parts. The "seed" energy U_{seed} is associated with the lattice of heavy ions and does not depend explicitly on the proton subsystem configuration. The pseudospin part of the Hamiltonian makes allowance for the short-range, $\hat{H}_{\text{short}}$, and long-range, $\hat{H}_{\text{MF}}$, proton-proton interactions near the HPO_3 tetrahedra, as well as the effective interaction with the electric fields E_1, E_2, and E_3. Hence,

$$\hat{H} = NU_{\text{seed}} + \hat{H}_{\text{short}} + \hat{H}_{\text{MF}} + \hat{H}_E, \tag{1}$$

where N is the total number of primitive cells in the Bravais lattice.

The quantity U_{seed} is the seed energy consisting of the elastic, piezoelectric, and dielectric components, which are expressed in terms of the electric fields E_i ($i = 1, 2, 3$) and the strains ε_j ($j = 1, 2, 3, 4, 5, 6$), so that

$$U_{\text{seed}} = v\Bigg(\frac{1}{2}\sum_{i,i'=1}^{3} c_{ii'}^{E0}(T)\varepsilon_i\varepsilon_{i'} + \sum_{i=1}^{3} c_{i5}^{E0}(T)\varepsilon_i\varepsilon_5 +$$
$$+ \frac{1}{2}c_{44}^{E0}(T)\varepsilon_4^2 + \frac{1}{2}c_{66}^{E0}(T)\varepsilon_6^2 + c_{46}^{E0}(T)\varepsilon_4\varepsilon_6 -$$
$$- \sum_{i=1}^{3} e_{2i}^{0}\varepsilon_i E_2 - e_{25}^{0}\varepsilon_5 E_2 - e_{14}^{0}\varepsilon_4 E_1 -$$
$$- e_{16}^{0}\varepsilon_6 E_1 - e_{34}^{0}\varepsilon_4 E_3 - e_{36}^{0}\varepsilon_6 E_3 -$$
$$- \frac{1}{2}\chi_{11}^{\varepsilon 0}E_1^2 - \frac{1}{2}\chi_{22}^{\varepsilon 0}E_2^2 - \frac{1}{2}\chi_{33}^{\varepsilon 0}E_3^2 - \chi_{31}^{\varepsilon 0}E_3E_1\Bigg). \tag{2}$$

Here, the parameters $c_{jj}^{E0}(T)$ are the so-called seed elastic constants, e_{ij}^0 the piezoelectric stress coefficients, $\chi_{ij}^{\varepsilon 0}$ the dielectric susceptibilities, and v the primitive cell volume.

The Hamiltonian of short-range interactions equals

$$\hat{H}_{\text{short}} = -2\sum_{qq'}\Big(w_1\frac{\sigma_{q1}}{2}\frac{\sigma_{q2}}{2} + w_2\frac{\sigma_{q3}}{2}\frac{\sigma_{q4}}{2}\Big)\times$$
$$\times\Big(\delta_{\mathbf{R}_q\mathbf{R}_{q'}} + \delta_{\mathbf{R}_q+\mathbf{R}_{\mathbf{c}},\mathbf{R}_{q'}}\Big), \tag{3}$$

where σ_{qf} ($f = 1, 2, 3, 4$) is the z-component of the operator for the pseudospin located at the f-th bond in the q-th cell; the first and second Kronecker deltas correspond to the proton interaction in the chains located near the HPO_3 tetrahedra of types I and II, respectively; and $\mathbf{R}_{\mathbf{c}}$ is the lattice radius vector directed along the c-axis. The contributions of the interaction between protons located around the tetrahedra of different types to the configuration energy are assumed to be identical, as well as the average values of pseudospins $\langle\sigma_{qf}\rangle$ related to the tetrahedra of different types. The quantitiesw_1 and w_2 describe short-range interactions of protons in the chains. We can expand them in series in the strains ε_j and confine the expansions to the linear terms,

$$w_{1,2} = w^0 + \sum_l \delta_l\varepsilon_l \pm \delta_4\varepsilon_4 \pm \delta_6\varepsilon_6 \quad (l = 1, 2, 3, 5). \tag{4}$$

The mean-field Hamiltonian $\hat{H}_{\text{MF}}$ describes long-range dipole-dipole interactions and indirect (through lattice vibrations) proton-proton interactions. Accounting for the expansion of the Fourier transforms of the interaction constants $J_{ff'} = \sum_{q'} J_{ff'}(qq')$ at $\mathbf{q} = 0$ in series in the strains ε_j and confining the expansions to the linear terms,

$$J_{\frac{11}{33}} = J_{11}^0 + \sum_l \psi_{11l}\varepsilon_l \pm \psi_{114}\varepsilon_4 \pm \psi_{116}\varepsilon_6,$$
$$J_{\frac{13}{24}} = J_{\frac{13}{24}}^0 + \sum_l \psi_{\frac{13l}{24l}}\varepsilon_l + \psi_{\frac{134}{244}}\varepsilon_4 + \psi_{\frac{136}{246}}\varepsilon_6,$$

$$J_{\frac{12}{34}} = J_{12}^0 + \sum_l \psi_{12l}\varepsilon_l \pm \psi_{124}\varepsilon_4 \pm \psi_{126}\varepsilon_6,$$

$$J_{\frac{14}{23}} = J_{14}^0 + \sum_l \psi_{14l}\varepsilon_l \pm \psi_{144}\varepsilon_4 \pm \psi_{146}\varepsilon_6,$$

$$J_{\frac{22}{44}} = J_{22}^0 + \sum_l \psi_{22l}\varepsilon_l \pm \psi_{224}\varepsilon_4 \pm \psi_{226}\varepsilon_6,$$

we obtain the term $\hat{H}_{\rm MF}$ in the form

$$\hat{H}_{\rm MF} = NH^0 + \hat{H}_s, \tag{5}$$

where

$$H^0 = \frac{1}{8}J_{11}(\eta_1^2+\eta_3^2) + \frac{1}{8}J_{22}(\eta_2^2+\eta_4^2) + \\ + \frac{1}{4}J_{13}\eta_1\eta + J_{24}\eta_2\eta_4 + \frac{1}{4}J_{12}(\eta_1\eta_2+\eta_3\eta_4) + \\ + \frac{1}{4}J_{14}(\eta_1\eta_4+\eta_2\eta_3) \tag{6}$$

and

$$\hat{H}_s = -\sum_q \left(\mathcal{H}_1\frac{\sigma_{q1}}{2} + \mathcal{H}_2\frac{\sigma_{q2}}{2} + \mathcal{H}_3\frac{\sigma_{q3}}{2} + \mathcal{H}_4\frac{\sigma_{q4}}{2}\right). \tag{7}$$

In formula (7), the following notations were used:

$$\mathcal{H}_f = \sum_{f'=1}^{4}\frac{1}{2}J_{ff'}\eta_{f'} \quad (f = 1\div 4).$$

The fourth term in Eq. (1), $\hat{H}_E$, describes the interaction of pseudospins with electric fields,

$$\hat{H}_E = \sum_{f=1}^{4} H_{Ef}\frac{\sigma_{qf}}{2}, \tag{8}$$

where

$$H_{E1,3} = \pm\mu_{13}^x E_1 + \mu_{13}^y E_2 \pm \mu_{13}^z E_3,$$

$$H_{E2,4} = \mp\mu_{24}^x E_1 - \mu_{24}^y E_2 \pm \mu_{24}^z E_3,$$

and $\mu_{13}^{x,y,z} = \mu_1^{x,y,z} = \mu_3^{x,y,z}$ and $\mu_{24}^{x,y,z} = \mu_2^{x,y,z} = \mu_4^{x,y,z}$ are effective dipole moments per pseudospin.

When calculating the thermodynamic and dynamic parameters of ferroactive compounds of the GPI type, let us apply the two-particle cluster (TPC) approximation. In this approximation, the thermodynamic potential of GPI under the action of the shear stresses $\sigma_{5,6}$ looks like

$$G = NU_{\rm seed} + NH^0 - N\upsilon\sum_{j=5}^{6}\sigma_j\varepsilon_j - \\ - k_{\rm B}T\sum_q\left[2\ln{\rm Sp}\, e^{-\beta\hat{H}_q^{(2)}} - \sum_{f=1}^{4}\ln{\rm Sp}\, e^{-\beta\hat{H}_{qf}^{(1)}}\right]. \tag{9}$$

Here, $\hat{H}_q^{(2)}$ and $\hat{H}_{qf}^{(1)}$ are the two- and one-particle, respectively, Hamiltonians given by the following expressions:

$$\hat{H}_q^{(2)} = -2\left(w_1\frac{\sigma_{q1}}{2}\frac{\sigma_{q2}}{2} + w_2\frac{\sigma_{q3}}{2}\frac{\sigma_{q4}}{2}\right) - \sum_{f=1}^{4}\frac{y_f}{\beta}\frac{\sigma_{qf}}{2}, \tag{10}$$

$$\hat{H}_{qf}^{(1)} = -\frac{\bar{y}_f}{\beta}\frac{\sigma_{qf}}{2}, \tag{11}$$

where the following notations were used:

$$y_f = \beta(\Delta_1 + \mathcal{H}_f + H_{Ef}), \quad \bar{y}_f = \beta\Delta_f + y_f.$$

The quantities Δ_f are effective fields created by neighbor links located beyond the cluster boundaries. In the cluster approximation, the fields Δ_f are determined from the self-consistency condition

$$\frac{{\rm Sp}\,\sigma_{qf}e^{-\beta\hat{H}_q^{(2)}}}{{\rm Sp}\,e^{-\beta\hat{H}_q^{(2)}}} = \frac{{\rm Sp}\,\sigma_{qf}e^{-\beta\hat{H}_{qf}^{(1)}}}{{\rm Sp}\,e^{-\beta\hat{H}_{qf}^{(1)}}}. \tag{12}$$

Then, on the basis of Eq. (12), we obtain expressions for the average values of the pseudospin, $\langle\sigma_{qf}\rangle$, in the cases of two- and one-particle Hamiltonians. By excluding the parameters Δ_f, we obtain the following relations:

$$\eta_{\frac{1}{3}} = \frac{1}{D}\Big[\sinh n_1 \pm \sinh n_2 + a^2\sinh n_3 \pm \\ \pm a^2\sinh n_4 + aa_{46}\sinh n_5 + \frac{a}{a_{46}}\sinh n_6 \mp \\ \mp aa_{46}\sinh n_7 \pm \frac{a}{a_{46}}\sinh n_8\Big],$$

$$\eta_{\frac{2}{4}} = \frac{1}{D}\Big[\sinh n_1 \pm \sinh n_2 - a^2\sinh n_3 \mp \\ \mp a^2\sinh n_4 \mp aa_{46}\sinh n_5 \pm \frac{a}{a_{46}}\sinh n_6 + \\ + aa_{46}\sinh n_7 + \frac{a}{a_{46}}\sinh n_8\Big],$$

$$D = \cosh n_1 + \cosh n_2 + a^2 \cosh n_3 +$$
$$+ a^2 \cosh n_4 + a a_{46} \cosh n_5 + \frac{a}{a_{46}} \cosh n_6 +$$
$$+ a a_{46} \cosh n_7 + \frac{a}{a_{46}} \cosh n_8,$$

where

$$a = \exp\left[-\beta\left(w^0 + \sum_{l=1}^{3} \delta_i \varepsilon_i\right)\right],$$
$$a_{46} = \exp\left[-\beta\left(\delta_4 \varepsilon_4 + \delta_6 \varepsilon_6\right)\right],$$
$$n_1 = \frac{1}{2}(y_1 + y_2 + y_3 + y_4),$$
$$n_2 = \frac{1}{2}(y_1 + y_2 - y_3 - y_4),$$
$$n_3 = \frac{1}{2}(y_1 - y_2 + y_3 - y_4),$$
$$n_4 = \frac{1}{2}(y_1 - y_2 - y_3 + y_4),$$
$$n_5 = \frac{1}{2}(y_1 - y_2 + y_3 + y_4),$$
$$n_6 = \frac{1}{2}(y_1 + y_2 + y_3 - y_4),$$
$$n_7 = \frac{1}{2}(-y_1 + y_2 + y_3 + y_4),$$
$$n_8 = \frac{1}{2}(y_1 + y_2 - y_3 + y_4),$$

and

$$y_f = \frac{1}{2} \ln \frac{1 + \eta_f}{1 - \eta_f} + \frac{\beta}{2} H_f + \frac{\beta}{2} \boldsymbol{\mu}_f \mathbf{E}.$$

3. Thermodynamic Parameters of GPI

In order to obtain the dielectric, piezoelectric, and elastic parameters of GPI, let us use formula (9) to calculate the thermodynamic potential per primitive cell,

$$g = \frac{G}{N} = U_{\text{seed}} + H^0 - 2\left(w^0 + \sum_l \delta_l \varepsilon_l\right) +$$
$$+ 2k_{\text{B}}T \ln 2 - N\upsilon \sum_{j=5}^{6} \sigma_j \varepsilon_j - \frac{1}{2} k_{\text{B}} T \sum_{f=1}^{4} \ln\left(1 - \eta_f^2\right) -$$
$$- 2k_{\text{B}}T \ln D, \quad l = 1, 2, 3, 5. \tag{13}$$

By differentiating this expression with respect to the fields E_i, we obtain the following formulas for the polarizations P_i:

$$P_1 = e_{14}^0 \varepsilon_4 + e_{16}^0 \varepsilon_6 + \chi_{11}^{\varepsilon 0} E_1 +$$
$$+ \frac{1}{2\upsilon}[\mu_{13}^x(\eta_1 - \eta_3) - \mu_{24}^x(\eta_2 - \eta_4)], \tag{14}$$
$$P_2 = e_{21}^0 \varepsilon_1 + e_{22}^0 \varepsilon_2 + e_{23}^0 \varepsilon_3 + e_{25}^0 \varepsilon_5 + \chi_{22}^{\varepsilon 0} E_2 +$$
$$+ \frac{1}{2\upsilon}[\mu_{13}^y(\eta_1 + \eta_3) - \mu_{24}^y(\eta_2 + \eta_4)], \tag{15}$$
$$P_3 = e_{34}^0 \varepsilon_4 + e_{66}^0 \varepsilon_6 + \chi_{33}^{\varepsilon 0} E_3 +$$
$$+ \frac{1}{2\upsilon}[\mu_{13}^z(\eta_1 - \eta_3) + \mu_{24}^z(\eta_2 - \eta_4)]. \tag{16}$$

The static isothermal dielectric susceptibilities along the axes of a mechanically clamped GPI crystal look like

$$\chi_{11}^{\varepsilon} = \chi_{11}^{\varepsilon 0} +$$
$$+ \frac{1}{2\upsilon}\left[\mu_{13}^x(\dot\eta_{1E_1} - \dot\eta_{3E_1}) - \mu_{24}^x(\dot\eta_{2E_1} - \dot\eta_{4E_1})\right], \tag{17}$$
$$\chi_{22}^{\varepsilon} = \chi_{22}^{\varepsilon 0} +$$
$$+ \frac{1}{2\upsilon}\left[\mu_{13}^y(\dot\eta_{1E_2} + \dot\eta_{3E_2}) - \mu_{24}^y(\dot\eta_{2E_2} + \dot\eta_{4E_2})\right], \tag{18}$$
$$\chi_{33}^{\varepsilon} = \chi_{33}^{\varepsilon 0} +$$
$$+ \frac{1}{2\upsilon}\left[\mu_{13}^z(\dot\eta_{1E_3} - \dot\eta_{3E_3}) + \mu_{24}^z(\dot\eta_{2E_3} - \dot\eta_{4E_3})\right], \tag{19}$$

where $\dot\eta_{1E}$, $\dot\eta_{3E}$, $\dot\eta_{2E}$, and $\dot\eta_{4E}$ are the solutions of the following system of equations:

$$\begin{pmatrix} 2D - \varkappa_{11} & -\varkappa_{12} & -\varkappa_{13} & -\varkappa_{14} \\ -\varkappa_{21} & 2D - \varkappa_{22} & -\varkappa_{23} & -\varkappa_{24} \\ -\varkappa_{31} & -\varkappa_{32} & 2D - \varkappa_{33} & -\varkappa_{34} \\ -\varkappa_{41} & -\varkappa_{42} & -\varkappa_{43} & 2D - \varkappa_{44} \end{pmatrix} \times$$
$$\times \begin{pmatrix} \dot\eta_{1E_\alpha} \\ \dot\eta_{2E_\alpha} \\ \dot\eta_{3E_\alpha} \\ \dot\eta_{4E_\alpha} \end{pmatrix} = \begin{pmatrix} \varkappa_1^{\chi\alpha} \\ \varkappa_2^{\chi\alpha} \\ \varkappa_3^{\chi\alpha} \\ \varkappa_4^{\chi\alpha} \end{pmatrix}. \tag{20}$$

Here, the following notations were used:

$$\varkappa_{f1} = \varkappa_{f11}(\varphi_1^+ + \beta\bar\nu_1^+) + \varkappa_{f12}(\beta\nu_2^+ + \beta\bar\nu_2^+) +$$
$$+ \varkappa_{f13}(\varphi_1^- + \beta\bar\nu_1^-) + \varkappa_{f14}\beta(\nu_2^- + \beta\bar\nu_2^-);$$
$$\varkappa_{f2} = \varkappa_{f12}(\varphi_2^+ + \beta\bar\nu_3^+) + \varkappa_{f11}(\beta\nu_2^+ + \beta\bar\nu_2^-) +$$
$$+ \varkappa_{f14}(\varphi_2^- + \beta\bar\nu_3^-) + \varkappa_{f13}(\beta\nu_2^- + \beta\bar\nu_2^+),$$
$$\varkappa_{f3} = \varkappa_{f11}(\varphi_3^+ - \beta\bar\nu_1^-) + \varkappa_{f12}(\beta\nu_2^+ - \beta\bar\nu_2^+) -$$
$$- \varkappa_{f13}(\varphi_3^- - \beta\bar\nu_1^+) - \varkappa_{f14}(\beta\nu_2^- - \beta\bar\nu_2^-),$$

$$\varkappa_{f4} = \varkappa_{f12}(\varphi_4^+ - \beta\bar{\nu}_3^-) + \varkappa_{f11}(\beta\nu_2^+ - \beta\bar{\nu}_2^-) -$$
$$- \varkappa_{f14}(\varphi_4^- - \beta\bar{\nu}_3^+) - \varkappa_{f13}(\beta\nu_2^- - \beta\bar{\nu}_2^+),$$
$$\varkappa_f^{\chi x} = \varkappa_{f13}\beta\mu_{13}^x + \varkappa_{f15}\beta\mu_{24}^x, \varkappa_f^{\chi y} =$$
$$= \varkappa_{f11}\beta\mu_{13}^y + \varkappa_{f12}\beta\mu_{24}^y, \varkappa_f^{\chi z} =$$
$$= \varkappa_{f13}\beta\mu_{13}^z + \varkappa_{f14}\beta\mu_{24}^z,$$

$$\varphi_{1,3}^{\pm} = \frac{1}{1-\eta_{1,3}^2} + \beta\nu_1^{\pm},$$
$$\varphi_{2,4}^{\pm} = \frac{1}{1-\eta_{2,4}^2} + \beta\nu_3^{\pm},$$
$$\varphi_{1,3}^{\pm} = \frac{1}{1-\eta_{1,3}^2} + \beta\nu_1^{\pm},$$
$$\varphi_{2,4}^{\pm} = \frac{1}{1-\eta_{2,4}^2} + \beta\nu_3^{\pm},$$
$$\nu_l^{\pm} = \nu_l^{0\pm} + \sum_{i=1}^{3}\psi_{li}^{\pm}\varepsilon_i + \psi_{l5}^{\pm}\varepsilon_5,$$
$$\bar{\nu}_l^{\pm} = \psi_{l4}^{\pm}\varepsilon_4 + \psi_{l6}^{\pm}\varepsilon_6,$$
$$\nu_1^{0\pm} = \frac{1}{4}(J_{11}^0 \pm J_{13}^0), \quad \psi_{1i}^{\pm} = \frac{1}{4}(\psi_{11i} \pm \psi_{13i}),$$
$$\nu_2^{0\pm} = \frac{1}{4}(J_{12}^0 \pm J_{14}^0), \quad \psi_{2i}^{\pm} = \frac{1}{4}(\psi_{12i} \pm \psi_{14i}),$$
$$\nu_3^{0\pm} = \frac{1}{4}(J_{22}^0 \pm J_{24}^0), \quad \psi_{3i}^{\pm} = \frac{1}{4}(\psi_{22i} \pm \psi_{24i}),$$
$$\varkappa_{\frac{1}{3}11} = (l_{1+3}^c + l_{5+6}^c) - \eta_{\frac{1}{3}}(l_{1+3}^s + l_{5+6}^s),$$
$$\varkappa_{\frac{1}{3}12} = (l_{1-3}^c \mp l_{7-8}^c) - \eta_{\frac{1}{3}}(l_{1-3}^s + l_{7+8}^s),$$
$$\varkappa_{\frac{1}{3}13} = \pm(l_{2+4}^c + l_{7+8}^c) - \eta_{\frac{1}{3}}(l_{2+4}^s - l_{7-8}^s),$$
$$\varkappa_{\frac{1}{3}14} = (\pm l_{2-4}^c - l_{5-6}^c) - \eta_{\frac{1}{3}}(l_{2-4}^s - l_{5-6}^s),$$
$$\varkappa_{\frac{2}{4}11} = (l_{1-3}^c \mp l_{5-6}^c) - \eta_{\frac{2}{4}}(l_{1+3}^s + l_{5+6}^s),$$
$$\varkappa_{\frac{2}{4}12} = (l_{1+3}^c + l_{7+8}^c) - \eta_{\frac{2}{4}}(l_{1-3}^s + l_{7+8}^s),$$

On the basis of relations (14)–(16), we obtain expressions for the isothermal coefficients of piezoelectric strains in GPI, e_{1j}, e_{2l}, and e_{3j}:

$$e_{1j} = \left(\frac{\partial P_1}{\partial\varepsilon_l}\right)_{E_1} =$$
$$= e_{2j}^0 + \frac{1}{2v}[\mu_{13}^x(\dot{\eta}_{1\varepsilon_j} - \dot{\eta}_{3\varepsilon_j}) - \mu_{24}^x(\dot{\eta}_{2\varepsilon_j} - \dot{\eta}_{4\varepsilon_j})],$$
$$(j = 4, 6), \qquad (21)$$

$$e_{2l} = \left(\frac{\partial P_2}{\partial\varepsilon_l}\right)_{E_2} =$$
$$= e_{2l}^0 + \frac{1}{2v}[\mu_{13}^y(\dot{\eta}_{1\varepsilon_l} + \dot{\eta}_{3\varepsilon_l}) - \mu_{24}^y(\dot{\eta}_{2\varepsilon_l} + \dot{\eta}_{4\varepsilon_l})], \qquad (22)$$
$$e_{3j} = \left(\frac{\partial P_3}{\partial\varepsilon_j}\right)_{E_3} =$$
$$= e_{3j}^0 + \frac{1}{2v}[\mu_{13}^z(\dot{\eta}_{1\varepsilon_j} - \dot{\eta}_{3\varepsilon_j}) + \mu_{24}^z(\dot{\eta}_{2\varepsilon_j} - \dot{\eta}_{4\varepsilon_j})],$$
$$(j = 4, 6). \qquad (23)$$

Here, $\dot{\eta}_{1\varepsilon_l}$, $\dot{\eta}_{2\varepsilon_l}$, $\dot{\eta}_{3\varepsilon_l}$, and $\dot{\eta}_{4\varepsilon_l}$ are the solutions of the following system of equations:

$$\begin{pmatrix} 2D-\varkappa_{11} & -\varkappa_{12} & -\varkappa_{13} & -\varkappa_{14} \\ -\varkappa_{21} & 2D-\varkappa_{22} & -\varkappa_{23} & -\varkappa_{24} \\ -\varkappa_{31} & -\varkappa_{32} & 2D-\varkappa_{33} & -\varkappa_{34} \\ -\varkappa_{41} & -\varkappa_{42} & -\varkappa_{43} & 2D-\varkappa_{44} \end{pmatrix} \times$$
$$\times \begin{pmatrix} \dot{\eta}_{1\varepsilon_l} \\ \dot{\eta}_{2\varepsilon_l} \\ \dot{\eta}_{3\varepsilon_l} \\ \dot{\eta}_{4\varepsilon_l} \end{pmatrix} = \begin{pmatrix} \varkappa_1^{e_l} \\ \varkappa_2^{e_l} \\ \varkappa_3^{e_l} \\ \varkappa_4^{e_l} \end{pmatrix}, \qquad (24)$$

where the following notations were applied:

$$\varkappa_f^{e_l} = \beta(\psi_{1l}^+\varkappa_{f11} + \psi_{2l}^+\varkappa_{f12})(\eta_1 + \eta_3) +$$
$$+ \beta(\psi_{2l}^+\varkappa_{f11} + \psi_{3l}^+\varkappa_{f12})(\eta_2 + \eta_4) +$$
$$+ \beta(\psi_{1l}^-\varkappa_{f13} + \psi_{2l}^-\varkappa_{f14})(\eta_1 - \eta_3) +$$
$$+ \beta(\psi_{2l}^-\varkappa_{f13} + \psi_{3l}^-\varkappa_{f14})(\eta_2 - \eta_4) +$$
$$+ 2\beta\delta_l(\rho_{f1} + \rho_{f2}),$$
$$\psi_{1l}^{\pm} = \frac{1}{4}(\psi_{11l} \pm \psi_{13l}), \quad \psi_{2l}^{\pm} = \frac{1}{4}(\psi_{12l} \pm \psi_{14l}),$$
$$\psi_{3l}^{\pm} = \frac{1}{4}(\psi_{22l} \pm \psi_{24l}),$$
$$\rho_{\frac{1}{3}1} = -2(l_{3\pm4}^s - \eta_{\frac{1}{3}}l_{3+4}^c),$$
$$\rho_{\frac{1}{3}2} = -l_{5+6}^s \pm l_{7-8}^s + \eta_{\frac{1}{3}}(l_{5+6}^c + l_{7+8}^c),$$
$$\rho_{\frac{2}{4}1} = 2(l_{3\pm4}^s + \eta_{\frac{1}{3}}l_{3+4}^c),$$
$$\rho_{\frac{2}{4}2} = \pm l_{5-6}^s - l_{7+8}^s + \eta_{\frac{1}{3}}(l_{5+6}^c + l_{7+8}^c),$$
$$\rho_{\frac{1}{3}j} = l_{5+6}^s \pm l_{7-8}^s + \eta_{\frac{1}{3}}(l_{5+6}^c - l_{7+8}^c),$$
$$\rho_{\frac{2}{4}j} = \mp l_{5-6}^s + l_{7+8}^s + \eta_{\frac{2}{4}}(l_{5+6}^c - l_{7+8}^c),$$

$$l^s_{3\pm4} = a^2 \sinh n_3 \pm a^2 \sinh n_4,$$
$$l^c_{3+4} = a^2 \cosh n_3 + a^2 \cosh n_4.$$

The molar entropy of the proton subsystem equals

$$S = \frac{R}{4}\Big\{-2\ln 2 + \sum_{f=1}^{4} \ln(1-\eta_f) + 2\ln D - \\ - 2\big\{\beta\nu_1^+(\eta_1+\eta_3)^2 + \beta\bar{\nu}_1^+\big[\eta_1(\eta_1+\eta_3) + \\ + \eta_3(\eta_1-\eta_3)\big] + 2\beta\nu_2^+(\eta_1+\eta_3)(\eta_2+\eta_4) + \\ + 2\beta\bar{\nu}_2^+(\eta_1-\eta_3)(\eta_2+\eta_4) + \beta\nu_3^+(\eta_2+\eta_4)^2 + \\ + \beta\bar{\nu}_3^+[\eta_2(\eta_2+\eta_4) + \eta_4(\eta_2-\eta_4)] + \\ + \beta\nu_1^-(\eta_1-\eta_3)^2 + \\ + \beta\bar{\nu}_1^-[\eta_1(\eta_1-\eta_3) + \eta_3(\eta_1+\eta_3)] + \\ + 2\beta\nu_2^-(\eta_1-\eta_3)(\eta_2-\eta_4) + \\ + 2\beta\bar{\nu}_2^-(\eta_1+\eta_3)(\eta_2-\eta_4) + \beta\nu_3^-(\eta_2-\eta_4)^2 + \\ + \beta\bar{\nu}_3^-[\eta_2(\eta_2-\eta_4) - \eta_4(\eta_2+\eta_4)]\big\} + \frac{4w}{TD}M\Big\}. \quad (25)$$

Here, R is the universal gas constant. The heat capacity of the proton subsystem in a GPI crystal at a constant pressure can be found by differentiating entropy (25).

4. Comparison of the Results of Numerical Calculations with Experimental Data

The values of some microscopic parameters are required to numerically calculate the temperature dependences of the dielectric and piezoelectric parameters of GPI. These are the parameter of the short-range interaction w^0; the parameters of long-range interactions $\nu_f^{0\pm}$ $(f = 1, 2, 3)$; the deformation potentials δ_i and $\psi_{fi}^{\pm}$ $(i = 1, ..., 6)$; the effective dipole moments μ_{13}^a, μ_{24}^a, μ_{13}^b, μ_{24}^b, μ_{13}^c, and μ_{24}^c; the "seed" dielectric susceptibilities $\chi_{ij}^{\varepsilon 0}$; the "seed" piezoelectric strain coefficients e_{ij}^0; and the elastic constants c_{ij}^{E0}.

In order to determine the required values, we used the experimental temperature dependences of the following physical parameters of GPI: $P_s(T)$ [8], $C_p(T)$ [9], $\varepsilon_{11}^{\sigma}$, $\varepsilon_{33}^{\sigma}$ [1], d_{21}, and d_{23} [10]. The volume of the primitive GPI unit cell was taken equal to $\upsilon_{0.0} = 0.601 \times 10^{-21}$ cm^3.

The optimal values obtained for the parameters $\tilde{\nu}_f^{0\pm} = \nu_f^{0\pm}/k_{\rm B}$ of long-range interactions are $\tilde{\nu}_1^{0+} = \tilde{\nu}_2^{0+} = \tilde{\nu}_3^{0+} = 3.065$ K and $\tilde{\nu}_1^{0-} = \tilde{\nu}_2^{0-} = \tilde{\nu}_3^{0-} = 0.05$ K. The parameter of the short-range interaction w_0 in the GPI crystal was calculated to equal to $w_0/k_{\rm B} = 800$ K. The optimal values found for the deformation potentials $\tilde{\delta}_i = \delta_i/k_{\rm B}$ are $\tilde{\delta}_1 = 500$ K, $\tilde{\delta}_2 = 600$ K, $\tilde{\delta}_3 = 500$ K, $\tilde{\delta}_4 = 150$ K, $\tilde{\delta}_5 = 100$ K, and $\tilde{\delta}_6 = 150$ K; and the optimal values for $\tilde{\psi}_{fi}^{\pm} = \psi_{fi}^{\pm}/k_{\rm B}$ are $\tilde{\psi}_{f1}^{+} = 93.6$ K, $\tilde{\psi}_{f2}^{+} = 252.5$ K, $\tilde{\psi}_{f3}^{+} = 110.7$ K, $\tilde{\psi}_{f5}^{+} = 22.7$ K, $\tilde{\psi}_{f4}^{+} = \tilde{\psi}_{f6}^{+} = \tilde{\psi}_{f4}^{-} = \tilde{\psi}_{f6}^{-} = 79.5$ K, $\tilde{\psi}_{f1}^{-} = \tilde{\psi}_{f2}^{-} = \tilde{\psi}_{f3}^{-} = \tilde{\psi}_{f5}^{-} = 0$ K.

The effective dipole moments in the paraphase are $\boldsymbol{\mu}_{13} = (0.4, 4.05, 4.3) \times 10^{-18}$ esu cm and $\boldsymbol{\mu}_{24} = (-2.3, -3.0, 2.2) \times 10^{-18}$ esu cm. In the ferrophase, the y-component of the first dipole moment equals $\mu_{13\rm ferro}^y = 3.82 \times 10^{-18}$ esu cm.

The values of the "seed" piezoelectric strain coefficients e_{ij}^0, the "seed" dielectric susceptibilities $\chi_{ij}^{\varepsilon 0}$, and the "seed" elastic constants c_{ij}^{E0} are as follows: $e_{ij}^0 = 0.0$ esu/cm^2, $\chi_{11}^{\varepsilon 0} = 0.1$, $\chi_{22}^{\varepsilon 0} = 0.403$, $\chi_{33}^{\varepsilon 0} = 0.5$, $\chi_{31}^{\varepsilon 0} = 0.0$, $c_{11}^{0E} = 269.1$ kbar, $c_{12}^{E0} = 145$ kbar, $c_{13}^{E0} = 116.4$ kbar, $c_{15}^{E0} = 39.1$ kbar, $c_{22}^{E0} = [649.9 - 0.4(T - T_c)]$ kbar, $c_{23}^{E0} = 203.8$ kbar, $c_{25}^{E0} = 56.4$ kbar, $c_{33}^{E0} = 244.1$ kbar, $c_{35}^{E0} = -28.4$ kbar, $c_{55}^{E0} = 85.4$ kbar, $c_{44}^{E0} = 153.1$ kbar, $c_{46}^{E0} = -11$ kbar, and $c_{66}^{E0} = 118.8$ kbar.

Now, let us consider how the thermodynamic parameters of the GPI crystal are changed, when the shear stresses σ_5 and σ_6 and the electric field E_1 are applied simultaneously. The main mechanism of the influence of the shear stresses σ_5 and σ_6 on the thermodynamic parameters of the GPI crystal is associated with a specific temperature behavior of the order parameters η_f at various stresses. The stress σ_5 in the XZ-plane of the crystal does not affect the symmetry of the parameters, which are only shifted along the temperature axis in this case. On the other hand, the action of the stress σ_6 in the XY-plane of the crystal leads to the relations $\eta_1 = \eta_2 \neq \eta_3 = \eta_4$. Furthermore, the order parameters become smeared, which testifies to the disappearance of the phase transition from the ferroelectric phase into the paraelectric one.

If the shear stress σ_6 is applied in the absence of the electric field (curves 6_0^2 in all figures), the crystal symmetry decreases, and two sublattices (chain A and chain B) become non-equivalent (see work [7]). As a result, the interactions between pseudospins become stronger in chain A and weaker in chain B. The enhancement of interactions in either sublattice at a cer-

tain stress σ_6 initiates a phase transition into the ferroelectric phase and elevates the temperature T_c. In the figures to follow, the curves marked with the numbers 5 and 6 correspond to the applied mechanical stresses σ_5 and σ_6, respectively, the superscripts indicate the stress values (in kbar units), and the subscripts mean the field strength magnitudes (in MV/m units).

The temperature dependences of the GPI crystal polarization P_2 at various values of the stress σ_5, σ_6 and the electric field strength E_1 are shown in Fig. 2 (left panel). The combined action of those factors only leads to a shift of the curve $P_2(T)$ along the temperature axis. The polarization curve corresponding to a field strength of 4 MV/m and the stress $\sigma_5 = 0$ (curve 5^0_4) is the most shifted toward low temperatures, whereas curve 5^2_0 is the most shifted toward high temperatures. The growth of the field strength E_1 shifts the curves $P_2(T)$ to the left from curve 5^0_0, and the growth of the stress σ_5 to the right from it.

If the stress σ_6 and the electric field E_1 are applied, the phase transition becomes smeared (Fig. 2, right panel). If only the field or the stress is applied, the polarization curves $P_2(T)$ – curves 5^0_4 and 5^2_0, respectively – are zeroed at the phase transition temperature. At the same time, the combined action of the field E_1 and the stress σ_6 results in the disappearance of the phase transition temperature and the phase transition smearing.

If the stress σ_6 and the electric field E_1 are applied to the crystal, the polarizations P_1 and P_3 are induced (Fig. 3). If only the stress σ_6 is applied, those polarizations are zeroed at the phase transition temperature. If only the field E_1 is applied or the stress σ_6 and the electric field E_1 are applied together, the polarizations P_1 and P_3 are smeared at this temperature.

Under the action of the stress σ_6 and the electric field E_1, the curves $P_1(T)$ are positive and increase with the temperature. Then they reach a maximum and, afterward, decrease. The polarizations P_3 in this case are negative. They at first decrease to a minimum and then increase as the temperature grows further. The simultaneous growth of the field and the stress leads to an increase of the polarization magnitude. The induced polarization P_3 is much larger than the polarization P_1 obtained at the same values of the stress σ_6 and the electric field E_1. The induced polarizations arise because two sublattices become non-equivalent under the action of the stress

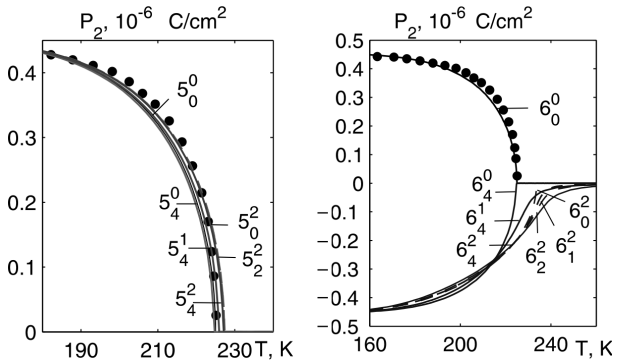

Fig. 2. Temperature dependences of the GPI crystal polarization P_2 at various values of the stresses σ_j and the electric field E_1

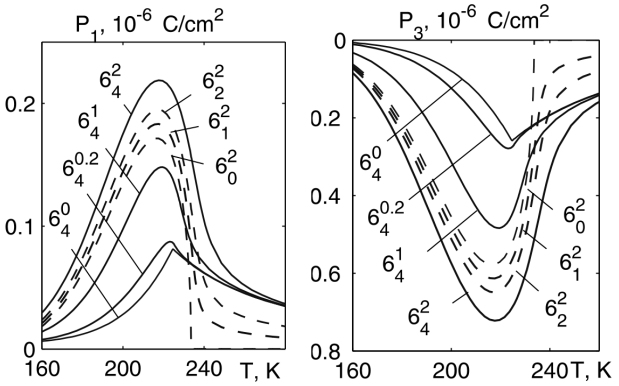

Fig. 3. Temperature dependences of the GPI crystal polarizations P_1 and P_3 at various values of the stress σ_6 and the electric field E_1

σ_6. Therefore, the dipole moments of two sublattices in the XZ and XY, respectively, planes are not compensated.

Figure 4 (left panel) demonstrates the temperature dependences of the inverse dielectric permittivity ε^{-1}_{22} of the GPI crystal, if the stress σ_5 and the electric field E_1 are applied. The combined action of those factors only shifts the $\varepsilon^{-1}_{22}(T)$ curves along the temperature axis. The growth of the field strength E_1 shifts the $\varepsilon^{-1}_{22}(T)$ curves to the left and the growth of the stress σ_5 to the right from curve 5^0_0. In the absence of the field and the stress, the longitudinal permeability diverges at the point T_c, but if they are applied, the maxima of ε_{22} become finite.

If the stress σ_6 and the electric field E_1 are applied to the crystal (Fig. 4, right panel), then curves 6^0_0, 6^0_2, and 6^4_0 for the inverse permeability ε^{-1}_{22} are zeroed at $T = T_c$. The combined action of the stress σ_6 and the

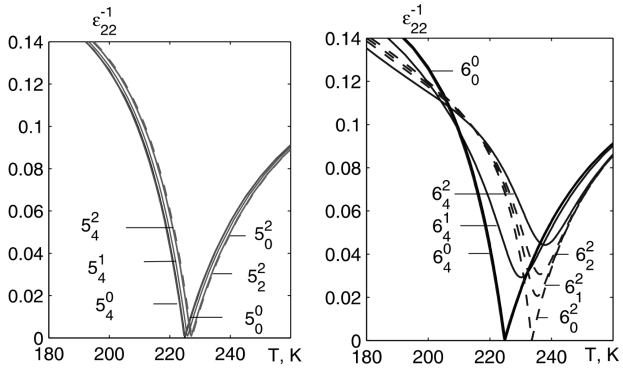

Fig. 4. Temperature dependences of the inverse dielectric constant ε_{22}^{-1} of the GPI crystal at various values of the stresses σ_j and the electric field E_1

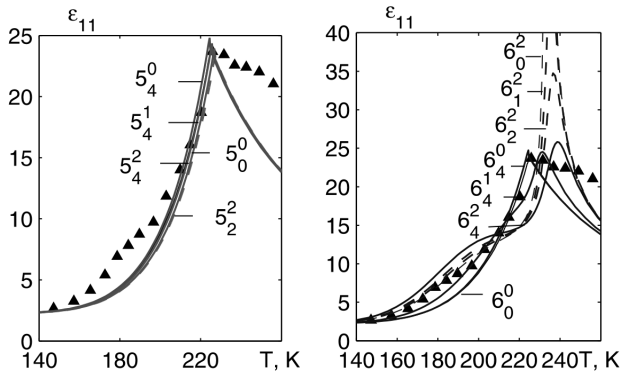

Fig. 5. Temperature dependences of the dielectric constant ε_{11} of the GPI crystal at various values of the stresses σ_j and the electric field E_1

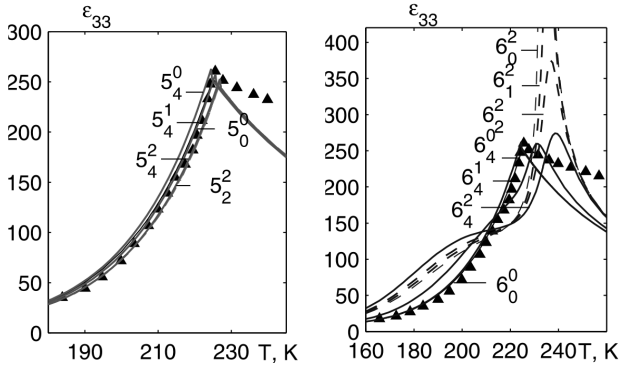

Fig. 6. Temperature dependences of the dielectric constant ε_{33} of the GPI crystal at various values of the stresses σ_j and the electric field E_1

field E_1 changes the permeability ε_{22}. In this case, the permeability ε_{22} decreases with the increasing stress at a constant field and with the increasing field at a constant stress.

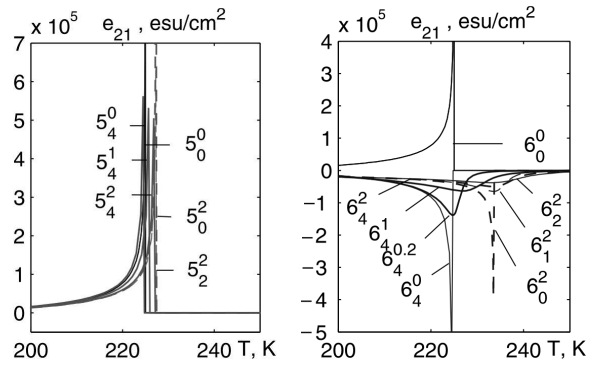

Fig. 7. Temperature dependences of the piezoelectric strain coefficient e_{21} of the GPI crystal at various values of the stresses σ_j and the electric field E_1

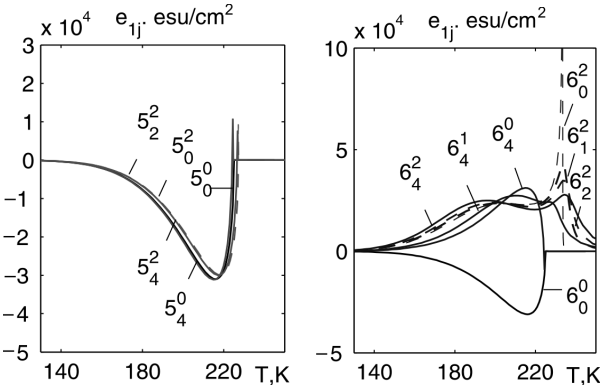

Fig. 8. Temperature dependences of the piezoelectric strain coefficient e_{1j} of the GPI crystal at various values of the stresses σ_j and the electric field E_1

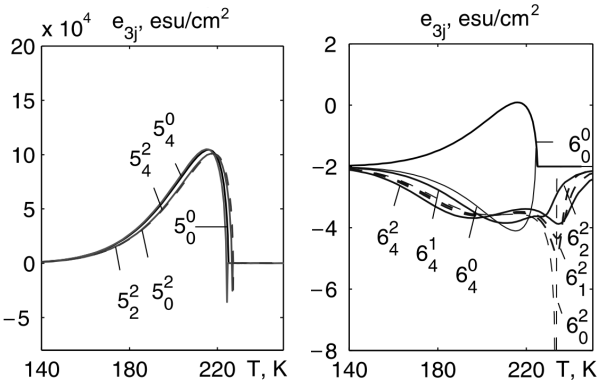

Fig. 9. Temperature dependences of the piezoelectric strain coefficient e_{3j} of the GPI crystal at various values of the stresses σ_j and the electric field E_1

If the stress σ_5 and the field E_1 are applied to the crystal, there arises a jump of the permittivities ε_{11} and ε_{33} at the phase transition temperature. These

jumps decrease and shift to higher temperatures with the growth of the stress σ_5 (Figs. 5 and 6). As was found in work [6], the reduction of T_c and the growth of ε_{33} in the ferroelectric phase occur due to a partial disordering of protons in the chain of type B (see Fig. 1) under the action of the field E_1.

If only the field E_1 is applied, each of the permeabilities ε_{11} and ε_{33} has a jump, and their maxima become smaller and more round as the stress σ_6 increases (Figs. 5 and 6). At the stress magnitudes exceeding 1 kbar, the curves $\varepsilon_{11}(T)$ and $\varepsilon_{33}(T)$ are smeared and there appear two maxima in them. If only the stress σ_6 is applied to the crystal, the permeability curves $\varepsilon_{11}(T)$ and $\varepsilon_{33}(T)$ behave as for the longitudinal permeability. The joint action of the stress σ_6 and the field E_1 makes the permeabilities ε_{11} and ε_{33} finite, and their values decrease with the increasing field.

The temperature dependences of the piezoelectric strain coefficient e_{21} for the GPI crystal under the action of the stress σ_5 and the field E_1 are shown in Fig. 7. If only the field E_1 is applied to the crystal, the curves $e_{21}(T)$ shift to lower temperatures and become finite. At the combined action of the stress σ_5 and the field E_1, the curves $e_{21}(T)$ shift toward higher temperatures as the stress σ_5 grows, and the negative e_{21}-maxima become some smaller.

The temperature dependences of the piezoelectric moduli e_{1j} (Fig. 8) and e_{3j} (Fig. 9) under the action of the stress σ_5 and the field E_1 are similar. At temperatures close to the phase transition one, the combined action of the stress σ_5 and the field E_1 leads to a drastic increase of the negative values of e_{1j} and the positive values of e_{3j}. At the combined action of the stress σ_6 and the field E_1, the curves for the piezoelectric moduli e_{1j} and e_{3j} are smeared, and the paraphase values of those parameters are induced. Another specific feature consists in the change of the signs of the transverse piezoelectric coefficients e_{1j} and e_{3j} near T_c, which is associated with an almost complete disordering of protons in chain B near T_c.

As one can see from Figs. 8 and 9 (curves 6_0^2), the temperature dependences $e_{1j}(T)$ and $e_{3j}(T)$ diverge at the T_c point. It occurs because, if the stress $\sigma_6 \neq 0$, small strain changes $d\varepsilon_4$ and $d\varepsilon_6$ are accompanied by a temperature change dT_c and a shift of the curves $P_1(T)$ and $P_3(T)$ to higher temperatures. Since $dP_i/dT \to \infty$ near the phase transition temperature, $dP_i/d\varepsilon_4 \to \infty$ and $dP_i/d\varepsilon_6 \to \infty$.

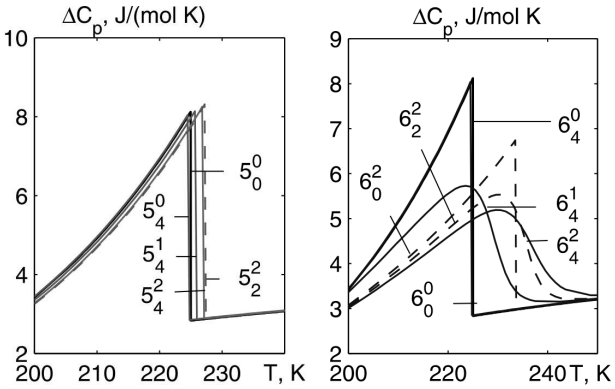

Fig. 10. Temperature dependences of ΔC_p of the GPI crystal at various values of the stresses σ_j and the electric field E_1

The temperature dependences of ΔC_p of the GPI crystal, when the stress σ_5 and the field E_1 are applied, are shown in Fig. 10 (left panel). In this case, the curves $\Delta C_p(T)$ become shifted toward lower temperatures and their maxima decrease. The reduction of the field E_1 leads to the growth of the $\Delta C_p(T)$ maximum.

If the stress σ_6 and the field E_3 are applied, the jump of ΔC_p becomes smeared as the stress σ_6 increases (Fig. 10, right panel).

5. Conclusions

In this work, the influence of the combined action of the stresses σ_5 and σ_6 and the electric field E_1 on the phase transition in and the physical parameters of the quasi-one-dimensional GPI ferroelectric has been studied. The research was performed in the framework of a modified model for the proton ordering in quasi-one-dimensional ferroelectrics with hydrogen bonds of the GPI type with regard for the piezoelectric coupling with the strains ε_j in the ferroelectric phase in the two-particle cluster approximation. It is found that the application of the shear stress σ_5 substantially increases the strain ε_5 and insignificantly the strain ε_3, whereas the stress σ_6 increases only the strain ε_6. It is also found that the action of the stresses σ_5 and σ_6 and the field E_1 affects the thermodynamic parameters of the GPI crystal by changing the temperature behavior of the order parameters.

The results of numerical calculations show how the changes in the temperature dependences of the thermodynamic parameters depend on the signs of the

stresses σ_j and the electric field E_1 under the combined action on those factors. In particular, if the stress σ_5 and the field E_1 are applied to the crystal, the temperature dependences of thermodynamic parameters become shifted along the temperature axis toward lower temperatures. The combined application of the stress σ_6 and the field E_1 results in the appearance of a number of interesting effects, e.g., the smearing of the polarization P_2 and the disappearance of the phase transition, the emergence of the transverse polarizations P_1 and P_3 in the ferroelectric and paraelectric phases, the emergence of the dielectric permittivity ε_{22} and the piezoelectric stress coefficient e_{21}, and the smearing of the piezoelectric strain constant h_{21}.

No additional parameters are used when carrying out the numerical calculations of thermodynamic parameters accounting for the shear stresses and the field E_1, as compared with the calculations performed for the case without the account for those external factors. Therefore, the temperature dependences obtained in this work for the thermodynamic parameters of the GPI crystal have a predictive character.

1. S. Dacko, Z. Czapla, J. Baran, M. Drozd. Ferroelectricity in Gly·H_3PO_3 crystal. *Phys. Lett. A* **223**, 217 (1996).
2. I. Stasyuk, Z. Czapla, S. Dacko, O. Velychko. Proton ordering model of phase transitions in hydrogen bonded ferrielectric type systems: the GPI crystal. *Condens. Matter Phys.* **6**, 483 (2003).
3. I. Stasyuk, Z. Czapla, S. Dacko, O. Velychko. Dielectric anomalies and phase transition in glycinium phosphite crystal under the influence of a transverse electric field. *J. Phys.: Condens. Matter* **16**, 1963 (2004).
4. I. Stasyuk, O. Velychko. Theory of electric field influence on phase transition in glycine phosphite. *Ferroelectrics* **300**, 121 (2004).
5. I.R. Zachek, Ya. Shchur, R.R. Levitskii, A.S. Vdovych. Thermodynamic properties of ferroelectric $NH_3CH_2COOH \cdot H_2PO_3$ crystal. *Physica B* **520**, 164 (2017).
6. I.R. Zachek, R.R. Levitskii, A.S. Vdovych, I.V. Stasyuk. Influence of electric fields on dielectric properties of GPI ferroelectric. *Condens. Matter Phys.* **20**, 23706 (2017).
7. I.R. Zachek, R.R. Levitskii, A.S. Vdovych. Deformation effects in glycinium phosphite ferroelectric. *Condens. Matter Phys.* **21**, 33702 (2018).
8. J. Nayeem, T. Kikuta, N. Nakatani, F. Matsui, S.-N. Takeda, K. Hattori, H. Daimon. Ferroelectric phase transition character of glycine phosphite. *Ferroelectrics* **332**, 13 (2006).
9. F. Shikanai, J. Hatori, M. Komukae, Z. Czapla, T. Osaka. Heat capacity and thermal expansion of $NH_3CH_2COOH \cdot H_2PO_3$. *J. Phys. Soc. Jpn.* **73**, 1812 (2004).
10. M. Wiesner. Piezoelectric properties of GPI crystals. *Phys. Status Solidi B* **238**, 68 (2003).

Received 10.01.20.
Translated from Ukrainian by O.I. Voitenko

А.С. Вдович, І.Р. Зачек, Р.Р. Левицький

ВПЛИВ НАПРУГ σ_5, σ_6 І ЕЛЕКТРИЧНОГО ПОЛЯ E_1 НА ТЕРМОДИНАМІЧНІ ХАРАКТЕРИСТИКИ СЕГНЕТОАКТИВНИХ МАТЕРІАЛІВ GPI

Для дослідження ефектів, що виникають під дією зовнішніх зсувних напруг σ_5, σ_6 і електричного поля E_1, використано модифіковану модель кристала GPI шляхом врахування п'єзоелектричного зв'язку структурних елементів, які впорядковуються, з деформаціями ε_j. В наближенні двочастинкового кластера розраховано вектори поляризації та компоненти тензора статичної діелектричної проникності механічно затиснутого кристала, їх п'єзоелектричні та теплові характеристики. Досліджено одночасну дію напруги σ_5 і поля E_1, а також напруги σ_6 і поля E_1 на фазовий перехід та фізичні характеристики кристала.

Ключові слова: сегнетоелектрики, фазовий перехід, діелектрична проникність, п'єзомодулі, зсувна напруга.